Study of jet engine plume phenomena on laser beam pointing and tracking

Work Package 2. TA108.019 Laser Beam Propagation and Imaging through severe Environments

MARKUS HENRIKSSON, DIRK SEIFFER, LARS SJÖQVIST,
RUY DERON, RIC (H.) M. A. SCHLEIJPEN

FOI, Swedish Defence Research Agency, is a mainly assignment-funded agency under the Ministry of Defence. The core activities are research, method and technology development, as well as studies conducted in the interests of Swedish defence and the safety and security of society. The organisation employs approximately 1000 personnel of whom about 800 are scientists. This makes FOI Sweden's largest research institute. FOI gives its customers access to leading-edge expertise in a large number of fields such as security policy studies, defence and security related analyses, the assessment of various types of threat, systems for control and management of crises, protection against and management of hazardous substances, IT security and the potential offered by new sensors.

FOI
Defence Research Agency
Information Systems
Box 1165
SE-581 11 Linköping

Phone: +46 13 37 80 00
Fax: +46 13 37 81 00

www.foi.se

FOI-R--2875--SE Technical report
ISSN 1650-1942 November 2009

Information Systems

Markus Henriksson, Dirk Seiffer, Lars Sjöqvist,
Ruy Deron, Ric (H.) M. A. Schleijpen

Study of jet engine plume phenomena on laser beam pointing and tracking

Work Package 2. TA108.019 Laser Beam Propagation and

Imaging through severe Environments

Titel	Studie av jetmotorplymfenomen på laserstrålstyrning och följning
Title	Study of jet engine plume phenomena on laser beam pointing and tracking
Rapportnr/Report no	FOI-R--2875--SE
Rapporttyp Report Type	Teknisk rapport
Sidor/Pages	28 p
Månad/Month	November
Utgivningsår/Year	2009
ISSN	ISSN 1650-1942
Kund/Customer	Försvarsmakten, FMV
Kompetenskloss	Telekrigssystem
Extra kompetenskloss	
Projektnr/Project no	E53051, E3098
Godkänd av/Approved by	Mikael Sjöman

FOI, Totalförsvarets Forskningsinstitut
Avdelningen för Informationssystem
Box 1165
581 11 Linköping

FOI, Swedish Defence Research Agency
Information Systems
Box 1165
SE-581 11 Linköping

Sammanfattning

Optiska system monterade på flygande plattformar kommer att störas av avgasutblåset från motorerna när de riktas bakåt. Den höga turbulensnivå som bildas när varma avgaser med hög hastighet blandas med den omgivande luften kan ge allvarliga begränsningar i prestanda hos systemen. Speciellt allvarligt är detta för skyddssystem som DIRCM (”Directed InfraRed Counter Measures”) som kan behöva peka nära eller delvis genom motorplymen för att skydda mot robotangrepp bakifrån.

För att studera dessa effekter har inom samarbetet TA108.019 en mätkampanj genomförts vid en nedskalad jetmotortestrigg på Volvo Aero i Trollhättan. Turbulenseffekterna mättes där genom att studera laserstrålar som propagerade längs och tvärs flödesriktningen från motorn.

Mätningarna visade att en laserstråle som propagerade längs motoraxeln beroende på motorpådrag och avstånd till motoraxeln ändrade riktning med upp till 350 μrad (rms). Detta är mer än vad som förväntas i atmosfären över relevanta avstånd och är tillräckligt för att ge en kraftig försämring av effektiviteten hos ett DIRCM-system. Med en fullskalig motor förväntas effekterna öka och störning av en robotmålsökare kan då troligen inte uppnås om systemet måste peka genom centrum på motorplymen.

Nyckelord: DIRCM, laser, turbulens, jetmotorer

Summary

Optical systems on aircraft will experience disturbances from the engine efflux when pointed backwards from the aircraft. The high level of turbulence, which is created when the hot exhaust leaving the engine at high speed is mixed with the surrounding air, may severely limit the performance of such systems. This is especially problematic for platform protection systems such as DIRCM (Directed Infra Red Counter Measures) that may need to point in the vicinity of, or through, the engine plume to protect against missile attacks from behind.

To study these effects the TA108.019 collaboration has performed a trial with a down-scaled (sub-scaled) jet engine test rig at Volvo Aero in Trollhättan. Turbulence effects were measured through study of laser beams passing along and across the engine flow axis.

The measurements showed that, depending on engine thrust and distance to engine axis, a laser beam propagating along the engine axis could be deflected by up to 350 μrad (rms). This is more than is expected in the atmosphere over relevant distances and may severely degrade the efficiency of a laser based DIRCM system in these conditions. With a full scale engine the effects are expected to increase and it is probable that jamming of a missile seeker through the center of the engine plume may be limited by taking longer for the jamming to be effective.

Keywords: DIRCM, laser, turbulence, jet engine

Contents

1 Introduction 7

2 Description of phenomena 8

3 Summary of previous work 9

4 Experiments 10

4.1 Description 10

4.2 Experimental arrangement....11

4.2.1 Laser propagation along engine axis....11
4.2.2 Laser propagation across engine axis....11
4.2.3 Tracking experiments....11
4.2.4 Wave front measurements....12

4.3 Results 13

4.3.1 Laser propagation along engine axis....13
4.3.2 Laser propagation across engine axis....15
4.3.3 Tracking experiments....16
4.3.4 Wave front measurements....17

4.4 Observations....20

5 Discussion on experimental techniques 23

6 Discussion regarding implications on system performance 25

7 Conclusion 27

References 28

1 Introduction

Refractive index variations in air, commonly discussed as turbulence, caused by variations in temperature, pressure and gas composition will cause refraction of a laser beam. Turbulence cells larger than the beam size mainly cause deflection while smaller turbulence cells distort the beam. These time-varying disturbances result in effects such as beam wander, beam broadening and scintillations. For atmospheric propagation there is a developed theory for predicting the order of magnitude and temporal statistics of the disturbances. In recent years there has been an increasing interest in mounting lasers on aircraft for applications such as directed infrared countermeasure systems (DIRCM), active imaging and optical communication.

Additional disturbances of the air originating from the aero-optical effects close to the fuselage of the aircraft and by the engine efflux then need to be considered. The turbulence caused by the hot exhaust gases from a jet engine will be much stronger than normal atmospheric turbulence and may show quite different spatial and temporal statistics. To be able to predict the performance of aircraft based laser systems in different pointing directions and the potential value of adaptive optical correction techniques it is important to characterize the turbulence caused by the jet engine. The area affected by the plume can be seen from the distortion of the trees in the background of Figure 1.

The project agreement TA108.019 “Laser beam propagation and imaging through severe Environments” between France, Germany, The Netherlands, Sweden and the United Kingdom was formed to evaluate the impact of aero-optical and turbulence effects on optical systems used on airborne platforms. This report is the final report for work package 2 “Study of jet engine plume and wake phenomena on laser beam pointing and tracking” and primarily discusses results and conclusions about laser beam propagation through and close to the engine plume from a field trial at Volvo Aero Corporation (VAC) in Trollhättan, Sweden in October 2007.

Figure 1. Gripen fighter during start. The upper limit of the area affected by the turbulence from the engine exhaust can be seen by the distortion of the trees in the background. Water droplets from the wet runway disturb the lower part of the image. (Photo: Peter Liander - Försvarets Bildbyrå)

2 Description of phenomena

In this section basic physical properties of relevance for turbulence effects and their influence on laser beam propagation are discussed. A review of the relevant phenomena and published work in the area was presented 2008 [1]. Turbulence properties within a jet engine plume are complicated to estimate from first principles and depend on several parameters such as variations in flow velocities, temperature and pressure distributions, mixture of exhaust gases and the geometrical properties of the engine nozzle. Considering laser beam propagation, the spatial and temporal variations in the refractive index are critical factors. The turbulent flow in a jet engine plume differs in spatial frequency content, turbulent length scales, the extent of the turbid region and temporal flow properties in comparison with atmospheric turbulence. Another issue which needs to be evaluated is the fact that the medium is anisotropic and non-homogeneous. All of this leads to a very complicated situation that cannot be modelled in a comprehensive way. Therefore, local isotropy and homogeneity is assumed as a first approximation in order to be able to adopt the formalism used to describe atmospheric turbulence.

Close to the nozzle there will be a quasi-laminar flow in the centre of the plume, whilst the shear stresses in the interface between the plume and the surrounding air will cause very high turbulence at the edge of the plume. Further away from the nozzle in the mixing region and the region were fully developed turbulence is present the turbulence on the engine axis will increase at the same time as the plume expands. The extent of the laminar flow region ends at approximately four to six nozzle diameters from the exit plane [2].

The common approach to describe turbulence strength is in terms of the refractive index structure constant C_n^2 and the inner and outer length scales, denoted l_0 and L_0 respectively. The inner- and outer scales are considerably smaller in the turbulent environment described by the jet engine exhaust in comparison with values observed in “atmospheric turbulence”. In plume regions typical values of L_0 range from 0.2 to 1 m[3], which is much smaller than atmospheric outer scales, which range from typically 10 to 100 m depending on altitude. The inner scale of turbulence is believed to be on the sub millimetre scale close to the engine. Because of the mixing of the hot exhaust with ambient atmosphere larger turbulence eddies are generated at longer distances from the nozzle.

3 Summary of previous work

Experimental studies on laser beam propagation through jet engine plumes have been reported by several groups. In the early study by Hogge and Visinski laser beam propagation parallel to an engine plume was used to estimate the averaged structure parameter describing the turbulence strength[4]. More recently laser beam propagation effects including beam broadening and wandering in strong turbulence with very high value of the structure parameter originating from the exhaust of a jet plume from a DeHavilland Vampire aircraft were studied[5]. The beam spreading and wander of visible and mid-IR laser beams propagating through a jet engine plume have been studied by using cameras to view and register perturbation effects[6].

The most comprehensive studies on laser beam propagation through jet engine plumes has been performed by Sirazetdinov and co-workers and was recently summarized in a journal paper[3], with a number of experiments described in references therein. They studied the influence from the plume on parameters such as beam wander and beam broadening for different laser wavelengths and propagation geometries. A dedicated experimental setup was described for studying both near- and far-field beam perturbation effects. Multi wavelength experiments using mid-IR lasers and fast imaging cameras studying beams crossing the plume close to the nozzle have also been reported by an Australian-British team[7, 8].

The experiments performed during 2007 in the TA108.019 group follows on two trials performed by FOI at the same test facility in 2003 and 2005. The 2003 trials were performed to gain an understanding of the phenomena and to learn how to perform measurements under the conditions at the jet engine test facility. Some results on laser beam wander and tracking of a black body source were reported[9]. During the 2005 trials a more thorough measurement of laser beam wander was performed. The results included magnitude and time statistics of the beam wander under a limited set of conditions[10].

The work of the TA 108.019 group introduces two important new contributions to the collective experimental data. The first contribution is that we have propagated the laser beam parallel to the jet engine plume at different distances from the engine axis, a case that is very relevant for the laser based DIRCM application, and studied the decline of the effects as we move away from the engine axis.

Secondly, a Shack-Hartmann wavefront sensor has been used to study the structure of the turbulence. In addition additional data was collected for phenomena that have already been described elsewhere, e.g. magnitudes and correlation times of laser beam wander and tracking of a blackbody source. Most of these data have been published in different parts earlier[11-14], but are summarized and put in a wider perspective in this report.

4 Experiments

4.1 Description

The experiments were performed using a down-scaled model jet engine located at Volvo Aero Corporation in Trollhättan, Sweden. The engine is designed to provide a characteristic exhaust in comparison with full-scale engines. Pressurized air is provided to the combustion chamber and optionally as a free streaming shear layer to simulate flight conditions. Air and fuel flows as well as the engine geometry can be varied to investigate different phenomena. The setup also includes sensors to monitor engine performance during the run. The engine used a circular nozzle with a diameter of 10 cm and the engine flow axis was situated approximately 1.1 m above the ground (Figure 2). The engine plume was enclosed with a roof and partial walls. In the flow direction a sound damping baffle was placed 8 m downstream of the nozzle. A larger hole was cut in the baffle to let that laser beams through so that they should not suffer any effects from shear layers at the baffle walls. During three days of trials in total eleven engine runs were made with different sensor combinations measuring the optical effects of the engine exhaust.

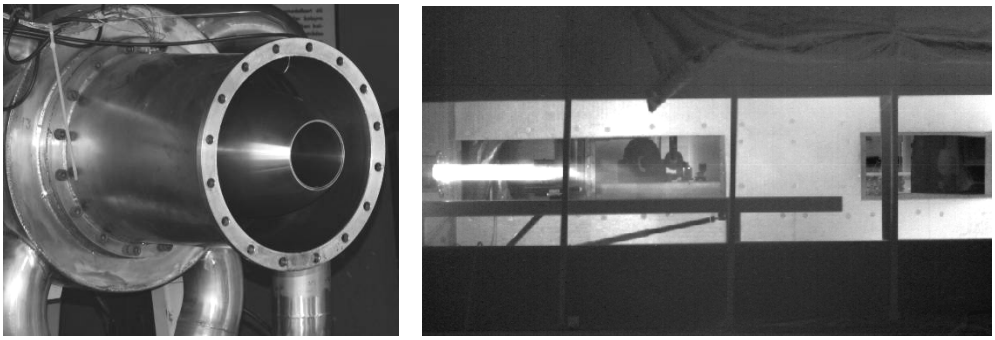

Figure 2. Down-scaled jet engine (left) and infrared image showing the running engine (right).

A number of different sensors were placed around the engine to collect as much data as possible. A schematical view of the setup for some of the sensors that were used is given in Figure 3.

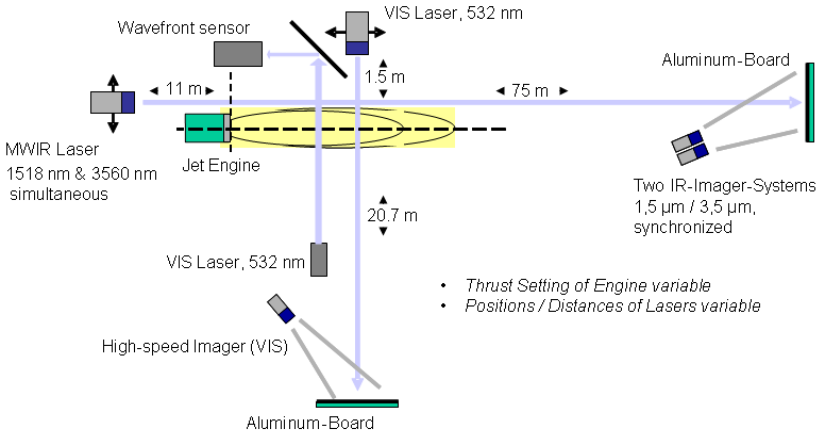

Figure 3. The sensor paths in the measurement setup.

4.2 Experimental arrangement

4.2.1 Laser propagation along engine axis

To study laser beam propagation along the engine axis a Nd:YVO_4 laser with a PPLN OPO emitting co-propagating signal and idler wavelengths of 1518 and 3560 nm was used. The laser was pulsed at the camera frame rate (100 Hz) and the pulse length was approximately 30 ns. The laser was placed on a tip-tilt mount and redirected by a mirror to adjust the position of the laser beam compared to the engine nozzle. The total path from the laser to the nozzle was 11 m. The distance from the nozzle to the laser beam was varied between 32 and 67 cm and the beam was approximately parallel to the engine axis. The closer distance was limited by the engine structure and the larger by the hole in the baffle.

The laser beams were projected on to an aluminium screen placed 75 m downstream from the nozzle. The laser spots were imaged by two separate cooled mercury-cadmium-telluride (MCT) arrays (AIM Infrarot-Module GmbH). The cameras used different filters so that one camera picked up only the 1.5 μm laser spot and the other only the 3.6 μm laser spot. The beam spots were slightly irregular because of thermal effects and the limited aperture in the PPLN crystal. Owing to the non-perfect beam quality the beam divergence was larger than the diffraction limit. At the laser aperture the e^{-2}-beam radius was approximately 2 mm for the 1.5 μm beam and 5×6 mm (elliptical half-widths) for the 3.5 μm beam.

At the screen the 1.5 μm beam spot was slightly elliptical with beam widths of 29 and 27 mm horizontally and vertically, respectively, (FWHM). Owing to the larger diffraction at the longer wavelength the 3.6 μm beam was somewhat larger with beam widths of 72 and 55 mm horizontally and vertically, respectively. The beam sizes when passing the engine plume where in the range 10-15 mm FWHM. The camera pixel size on the screen was 1.06 mm.

4.2.2 Laser propagation across engine axis

A corresponding measurement was made with the laser beam crossing the engine plume. For this experiment a continuous wave green laser (second harmonic of a Nd:YAG laser) was used. The laser beam crossed the engine plume 190 and 405 cm, respectively, from the nozzle in two different configurations. In both cases the beam was placed at the same height above ground as the engine nozzle. In the measurements a collimated laser beam with diameter approximately 2 mm was used. After crossing the jet plume the laser beam propagated 20.7 m to an aluminium screen. The laser spot on the screen was imaged by a high frame rate camera (Redlake Inc.). Exposure times from 10 to 994 μs and frame rates from 1000 to 5000 kHz where used in different runs. Each camera pixel corresponded to 0.22 mm on the screen.

4.2.3 Tracking experiments

Using a Thermacam-camera situated next to the mid-IR laser the 3.6 μm laser spot and a black body source situated above the target screen were imaged to study the effects of the plume from a tracking point of view. The camera studied both the situation of single pass through turbulence from the blackbody and double passage of the laser beam in the forward direction and the image of the laser spot in the return direction. The camera IFOV was 0.5 mrad.

4.2.4 Wave front measurements

A Shack Hartmann set-up for measuring the wave front degradation of light passing perpendicularly through the exhaust plume was used to characterize the smaller turbulence scales. The measurement system was set on two optical benches installed on either side of the exhaust plume axis. A spatially filtered laser source emitted collimated light towards the plume. The laser used was a Nd:YAG laser, frequency doubled to 532 nm, 40 Hz PRF, 15 ns pulse length and 2 μJ pulse energy. After passing the plume a flat mirror redirected the laser beam towards the receiving optics. The optical "receiver" was composed of a two lens telescope that focused and reduced the incoming beam to the size of the wave front sensor. The second lens of the collecting system was positioned on the optical axis such that it also conjugates the analysis plane of the wave front sensor with the plume region to be analyzed. The system utilizes the same common optical path arrangement for calibration and for turbulent measurements and this optical path arrangement was maintained in proper alignment under test conditions.

The Shack-Hartmann (S-H) wavefront sensing method is widely used for sensing atmospheric turbulence, but also more recently for flow diagnostics. The S-H sensor splits incoming collimated laser light into a number of small beams using an array of 64 by 64 lenslets each 190 μm in diameter. The light from each of these lenslets is focused on to a Dalsa CCD camera comprising 1024 by 1024 pixels. As the portion of the wavefront hitting the lenslet is aberrated, the focused spot on the CCD camera moves. Through simple geometry using the displacement of the focused spot and the focal length of the lenslet, the local tilt of the wavefront can be derived. The analyzer measures a combination of the aberrations in the input wavefront itself and the aberrations introduced by the different lenses of the optical system. By doing reference measurements before the engine is turned on the system aberrations can be subtracted and the aberrations that are introduced by the engine plume isolated.

The laser beam crossed the engine plume at two different distances downstream the engine nozzle (1142 mm and 3500 mm) and at the same height, 80 mm, above the plume main axis. Because of mechanical constraints, the optical set-up realized at VAC did not allow variation of the beam height. The two distances were supposed to provide data with different turbulent conditions: strong turbulent conditions and less severe ones. The 3500 mm distance was reached by slightly tilting the beam path from the optical emission point.

The optical beam was collimated to a 40 mm diameter given a physical analyzing size of 0.8 mm for each lenslet. Without any a priori knowledge about the nature and about the spatial characteristics of the plume turbulence, this diameter value was chosen in order to get a good sensitivity in the measurements of plume effects for the mid-range turbulent scales. Measurements of the influence of the outer and inner scales of the turbulence were not directly pursued in this first series of experiments because of the lack of knowledge of the order of magnitude of these two parameters. Actually a measurement of the large scale L_0 using a Shack-Hartmann analyzer would have required a much larger analyzing pupil lens if we consider the size of the turbulent plume at VAC (few tens of centimetres) and, at the same time, a measurement of the influence of the inner scale on the contrary a much smaller physical pupil. The instantaneous Shack-Hartmann images were turbulence frozen by using the pulsed laser with a 15 ns pulse length, synchronized with the SH sensor acquisition rate. For each downstream distance and engine run status investigated, a sequence of 270 couples of instantaneous local slope maps of the wave front was acquired by the Shack-Hartmann analyzer. But because of the limited frame rate of the Shack-Hartmann sensor at 40 Hz, the slope maps recorded during each run were completely uncorrelated in time.

4.3 Results

4.3.1 Laser propagation along engine axis

The mid-IR beams that propagate parallel to the jet engine plume at distances of a few nozzle diameters from the engine axis experience both tip-tilt aberrations, which cause beam wander, and higher order aberrations that cause distortion of the beam profile, such as beam break-up. As seen from Figure 4 the distortion is much more severe for the 1.5 µm beam (left) than for the 3.6 µm beam (right). The 1.5 µm beam is severely broken up for all conditions tested in this trial, while it is possible to see how the 3.6 µm beam deteriorates with increasing engine thrust. The difference is expected as scintillation effects scale inversely with the wavelength, causing more perturbations at shorter wavelengths.

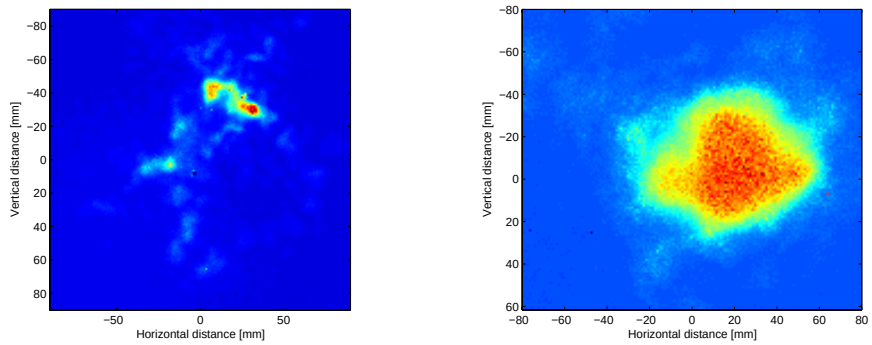

Figure 4. Examples of single laser pulses when the engine is running. To the left the 1.5 µm beam and to the right the 3.6 µm beam, respectively. The origin is defined as the average centroid position.

In the left part of Figure 5 the beam deviations from the average position for the 1.5 and 3.6 µm beams are plotted, synchronized in time. The small differences in the two traces can be explained by a slight difference in beam diameter when passing the plume and by influence of camera noise. Wavelength dependence of the centroid motion cannot be ruled out, but would have to be very small. This result is in agreement with the case for the free atmosphere. As the measurement is made with a time resolution of 10 ms the beam position between consecutive points is almost uncorrelated. The right part of Figure 5 shows the distribution of the vertical deviations from the average position. The distribution is similar to a Gaussian function. The maximum measured beam deviations are on the same order of magnitude as the beam sizes at the screen.

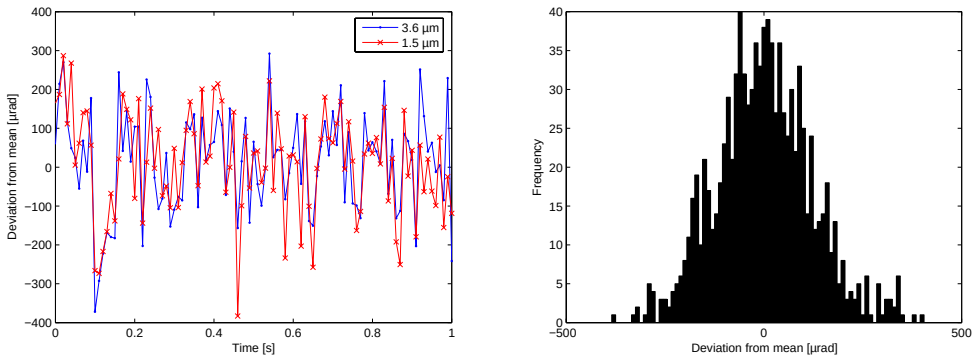

Figure 5. Left: variation over time of horizontal centroid positions for 1.5 µm and 3.6 µm beams. Right: Histogram of vertical centroid position of the 1.5 µm beam for 1000 laser pulses.

The dependence of the beam wander on the engine thrust is shown in the left part of Figure 6. Data points are provided for centroid motion and for the motion of the most intense peak for both wavelengths. There is a clear increase in the beam wander as the engine thrust is increased. As only three different engine settings were used no conclusions can be drawn on the functional dependence, but it seems like fitting a linear dependency is possible in the limited range of our measurement points. In the right part of Figure 6 the rms beam wander is plotted as a function of the distance between the engine axis and the laser beam. The distance was varied from slightly above three to almost seven nozzle diameters. The data were collected at full nominal thrust. A significant decrease in the beam wander is observed when the beam is moved away from the engine axis. The measured centroid rms beam wander varies from 75 to 228 µrad for different geometries and engine conditions.

As can be expected from the character of the laser spots in Figure 4 the movement of the highest peak is larger for the 1.5 µm beam than for 3.6 µm even if the centroid motions are the same. The difference is especially large at low thrust and decreases as the engine thrust increases. This is also reasonable since the 3.6 µm beam gets more distorted as the thrust increases.

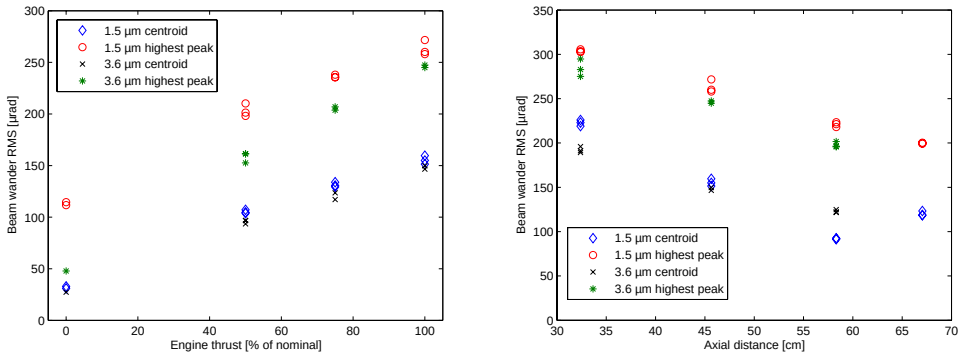

Figure 6. Root-mean-square (RMS) beam wander for laser beams propagating parallel to the engine axis. Left as a function of engine thrust and right as a function of the distance between the engine axis and the laser beam.

During the 2005 trials similar measurements were performed with camera settings that allowed 607 Hz frame rate with lower spatial resolution to image a 3.5 µm beam after passing along the plume[10]. This allowed the time dynamics of the beam centroid motion to be studied. The result of calculating the autocorrelation of the beam wander and averaging over all measurements is shown in Figure 7. The measurements with the engine on show a 50 % correlation time of 3.5 ms, which is slightly more than twice the time between two consecutive samples.

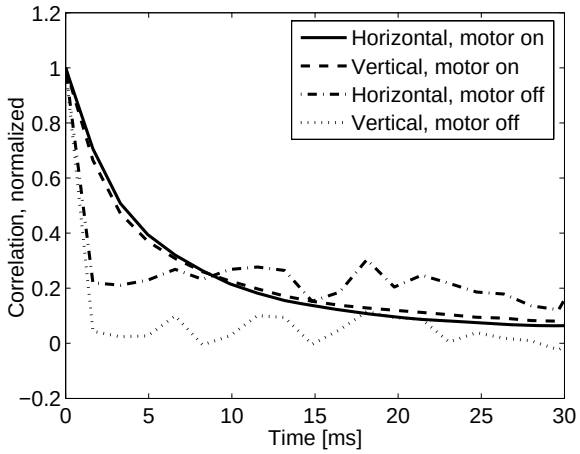

Figure 7. Normalized autocorrelation of the beam centroid position in the 2005 measurements.

4.3.2 Laser propagation across engine axis

In the left part of Figure 8 rms values of the beam wander are plotted versus the engine thrust. The difference between the two positions for crossing the plume is relatively small. The movement seems slightly larger in the vertical than in the horizontal direction. Even though asymmetry would not be unexpected as the laser beam propagates perpendicular to the flow direction experimental conditions may have a larger influence, and the difference in the data is not significant. The high-speed camera was looking on to the screen under a certain horizontal angle all dimensions, and therefore, also the wander in horizontal direction are reproduced slightly smaller. In addition the undisturbed laser beam was slightly elliptical, something that also influences the beam wander. The collected sequences show rms-beam wander values ranging from 50 to 120 µrad with a seemingly linear increase with the engine thrust.

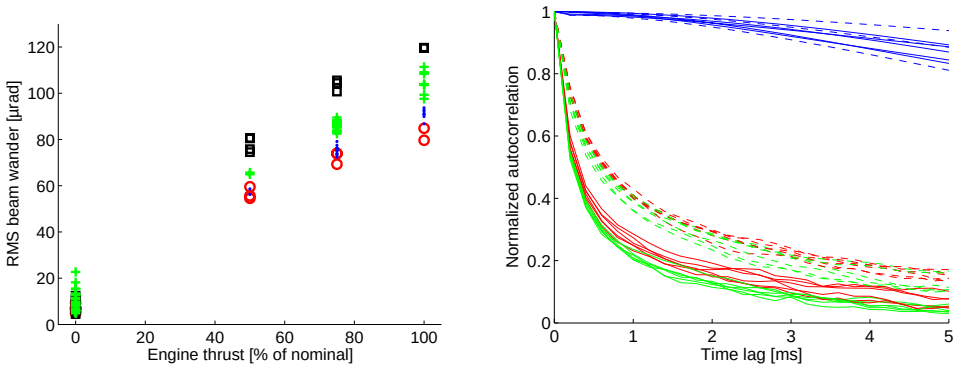

Figure 8. Left: Horizontal rms-beam wander of the green laser beam after crossing the engine plume. Red circles and black squares are horizontal and vertical data 1.9 m from the engine while blue dots and green pluses are corresponding data 4.05 m from the nozzle. Right: Autocorrelation of beam centroid position. Solid and dashed lines are horizontal and vertical directions respectively. Measurements with engine off [blue], at 75 % of nominal power [red] and at full power [green] are compared.

The time correlation of the beam wander was studied with the camera running at 5 kHz frame rates and exposure times from 10 to 20 µs. Fast frame-rate measurements were only performed with the laser beam crossing the plume 4 m from the nozzle. The normalized auto-correlation curves for these measurements are shown in the right part of Figure 8.

The data collected with the engine off show that beam wander from atmospheric turbulence and system noise varies at a slower timescale than the engine induced beam wander. Correlation times (50 % value) of 200-300 µs were found in the horizontal direction, while the values in the vertical direction were 500-700 µs. A small difference can be seen between the 75 % engine thrust and full engine thrust, with the correlation time decreasing with increasing thrust. The anisotropy is not surprising, as the air flow is in the direction of the faster movement.

4.3.3 Tracking experiments

The results of tracking through the plume were reported in [14]. Figure 9 illustrates the vertical displacement of the observed position of the black body in the camera image as a function of time for a typical run. The units for the vertical scale are in pixel size, corresponding to 0.5 mrad per pixel. The horizontal axis gives the frame number and covers roughly 40 s. The red curve shows the actual measured position, whereas the blue curve shows the moving average of the position. As the frame rate is 25 Hz there is no frame to frame correlation for the position.

In Figure 9 the results for three different engine settings are observed. Around image number 13000, the engine is started at an intermediate setting and the average observed black body position moves down 0.8 pixels. At 21000 the engine power is set to maximum and a further shift towards an observed position of 1 pixel away from the undisturbed position is observed. Finally, around image 27000, the airstream around the plume is switched on to simulate flight conditions and the observed black body position moves back to 0.5 pixels away from the undisturbed position. When the engine stops around 33000 the observed position moves back to 0.3 pixels above the undisturbed position. This indicates that the set-up of the camera has moved during the measurements. The actual maximum shift in observed position is therefore probably even slightly more than one pixel. The average effect is a shift up to 0.5 - 0.7 mrad of the observed black body position.

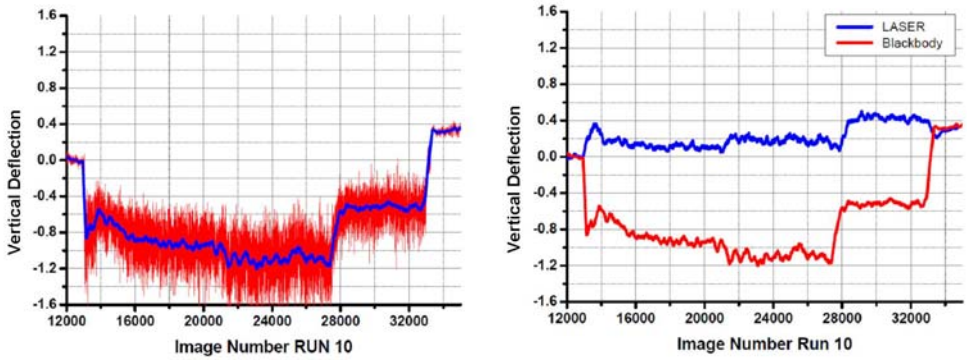

Figure 9. Left: Apparent deflection of blackbody, in red single frame positions and in blue moving average. Right: Comparison of apparent deflection of blackbody and of laser spot as viewed through plume.

Interestingly, the shift in the time averaged observed laser spot position is much smaller than the shift in the observed black body position, as can be seen in Figure 9. The fact that the shift of the laser spot appears smaller is a result of the fact that both the laser propagation path and the observation path are affected by the refraction in a similar way. However the refraction effects in both paths do not cancel each other completely, but a remaining shift of approximately 0.1 mrad can be found. Exact measurements were impossible because of the shift of the camera position during the run.

From the camera images that were used to study the beam wander, an upward deflection of the average position of 0.2 to 0.8 mrad was found depending on the distance to the engine

axis and the engine status. The engine run that was used for the tracking experiments through the plume was the one where the laser was at its closest to the engine axis. Compared with the tracking experiments this was not angle of arrival, but deflection angle calculated as if all refraction happened in a plane at the nozzle.

4.3.4 Wave front measurements

A short summary of the results obtained from the Shack Hartmann sensor is reported here, with the detailed results available in [12]. Figure 10 shows examples of instantaneous reconstructed wave fronts. The figures illustrate how optical wavefront aberrations look like when crossing the plume one meter downstream the engine nozzle and how predominant the overall tilt component fluctuations are, getting even worse with an increasing engine thrust.

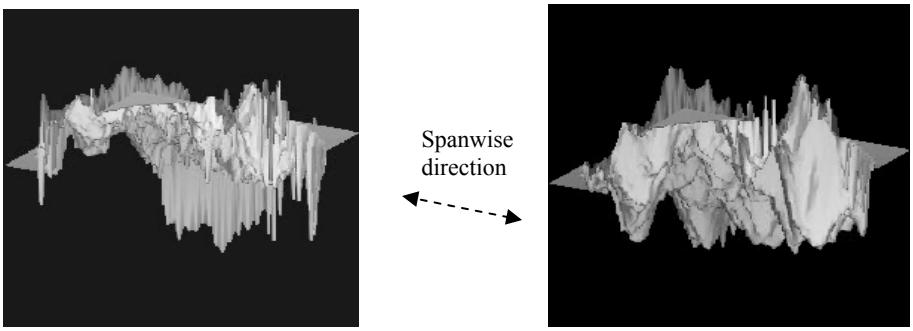

Figure 10. Instantaneous wavefronts for the position 1142 mm from the nozzle with engine run status 75 %. Left global wave front, and right the same wavefront with tilt removed. The rms fluctuations were 160 rad including the tilt and 30 rad without the tilt.

Figure 11 shows (top left) a typical example of the global wave front degradation, obtained after ensemble-averaging the 270 reconstructed wave front acquired at the position 1142 mm downstream the engine nozzle. After removing the overall averaged tilt component wave front exhibits a rather strong astigmatism effect (top right).

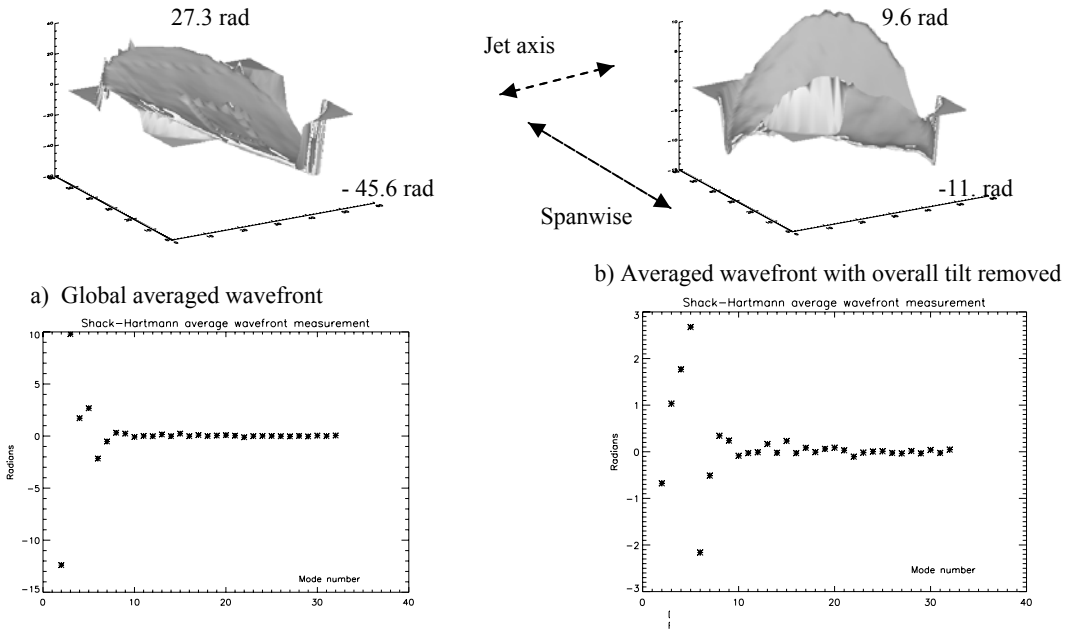

Figure 11. Turbulent averaged wavefront recorded at the position 1142 mm downstream the nozzle. Wave fronts are decomposed into the 32 first Zernike modes.

Wave front Zernike's decomposition up to the 32th polynom yields an amplitude of the order of ±10 radians for the tilt components, which represent the prevailing perturbation effect induced by traversing the plume. After removing the overall tilt component, Zernike's modes up to the 9th are the most relevant ones. The wave front quality suffers then essentially from defocus, astigmatism, with the highest amplitudes, and coma aberrations as can be noticed in the Zernike's wave front decomposition shown in the bottom right of the figure. The remaining higher modes are much smaller in comparison to the first nine modes.

In Figure 12, a quick comparison of all the results obtained at the two positions and for all the engine run conditions reveals a net difference concerning the amplitudes. The amplitudes at the position 3500 mm from the nozzle never exceed ±0.5 radians, whereas at the closer distance the amplitude of some lower modes goes up to 4 radians.

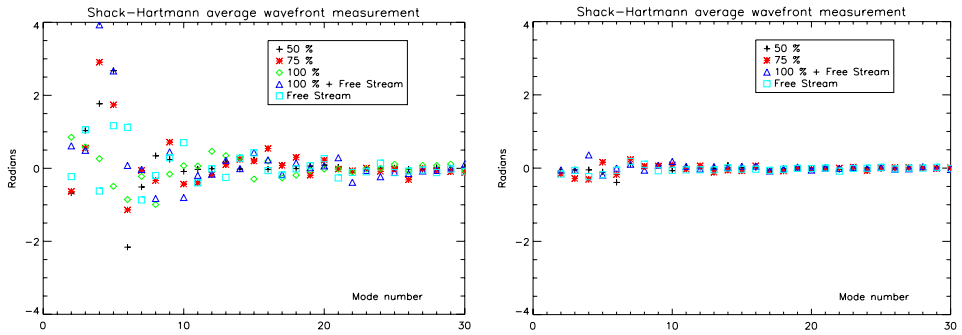

Figure 12. Wave front measurements obtained for the various aircraft turbine engine status experimented at distances of 1142 mm and 3500 mm downstream the engine nozzle. Wave fronts decomposed into the 32 first Zernike modes.

The rms wave front error and the power spectral densities of the perturbed optical phases were derived by performing statistical computations on each sequence acquired per engine run condition and composed of hundreds of reconstructed wave fronts.

The instantaneous wave fronts are aberrated unsymmetrically as it could be expected because of the jet speed, which drives the large turbulent structures away along the plume main axis. Statistical analysis results on the global rms wave front degradations are summarized in the Table 1. At the position about one metre downstream the engine nozzle the statistics were performed both by considering the global wave fronts and the wave fronts with the overall tilt component removed. The results obtained clearly show the main contribution of the overall tilt component in the wave front perturbation. Statistics performed on sets of reconstructed wave fronts with overall tilt removed show a difference of the rms optical degradations of four to five times smaller between the two distances from the engine nozzle. Under any given plume condition, overall tilt aberration prevails.

Table 1. Turbulent wavefront global root mean square obtained at the two positions 1142 mm and 3500 mm away from the engine nozzle

	Distance downstream the engine nozzle	**Wave front**	**Air Turbine Engine Status**			
			50%	75%	100% and Free Stream	Free Stream only
Wave Front r.m.s.	1142 mm	With Tilts	63,6 rad	156,8 rad	217,4 rad	27,8 rad
	1142 mm	Overall Tilt removed	11,7 rad	31 rad	37 rad	4,1 rad
	3500 mm	Overall Tilt removed	4,6 rad	6,3 rad	6 rad	1,3 rad

.

Table 1 summarizes the power spectral density (PSD) results derived from the sequences of Shack-Hartmann images acquired at the two different positions and for the five engine run conditions experimented. These PSDs results with overall tilt component removed are shown in Figure 13.

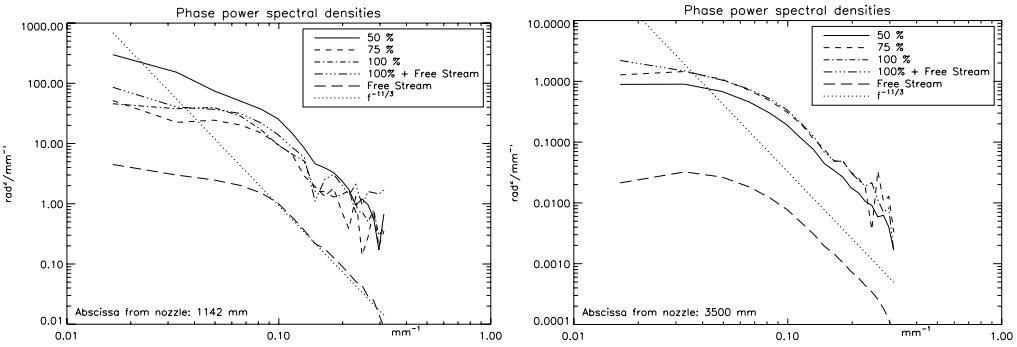

Figure 13. Turbulent wavefront Power Spectral Densities1142 mm (left) and 3500 mm (right) downstream the nozzle.

At the first position, 1142 mm downstream the engine nozzle, the amplitudes of the different curves scale according to the air turbine engine run status performed, except for the 50% condition where a higher degradation effect is evident particularly in the lower wave number range compared with the other engine run conditions. With the free stream air turbine condition, the PSD result drops roughly one decade in amplitude. The "free stream only" engine status corresponds by far to the less perturbed condition for an optical transmission through the plume, which is also expected as there is no combustion in this case. In general, the curve shapes compare well with the Kolmogorov -11/3 power law within a wave number domain ranging from 0.1 mm^{-1} up to 0.3 mm^{-1}.

Between the two positions, 1142 mm and 3500 mm downstream the engine nozzle, wave front degradation statistics drop, in general, by almost two decades in amplitude. Engine runs at 75%, 100% and or at 100% with free stream air conditions provide quite similar PSD amplitudes, considering the uncertainty in the experimental determination of the PSDs. Error estimation is difficult because of the small amount of valid wave front data acquired during the experiment at VAC.

4.4 Observations

For weak turbulence the beam centroid deviation from the average position resulting from beam wander can be approximated as [15]

$$\left\langle \rho_c^2 \right\rangle = \frac{2.97L^2}{k^2 \rho_0^{5/3} D^{1/3}} = \frac{4.34L^2}{D^{1/3}} \int_0^L C_n^2(\eta)\left(1-\frac{\eta}{L}\right)^{5/3} d\eta \qquad (1)$$

where ρ_c is the centroid deviation from the average position, ρ_0 is Fried's parameter, D is a measure of the beam diameter at the source, C_n^2 is the refractive index structure constant and η goes from 0 at the source to L at the screen. The validity of this expression for the strong turbulence in the engine plume and for broken up beams may be doubted, but it is useful as a first order approximation.

The definition of C_n^2 demands that the index of refraction has a slowly varying mean and that the fluctuations are locally homogenous and isotropic. It is not even evident that these conditions are fulfilled, but we choose to handle the situation as if a slowly varying structure parameter can be defined. If we assume that the structure parameter has a low constant value over most of the propagation path and a several orders of magnitude higher value in a short region where the beam passes the plume we can approximate this as $C_n^2 = C_{n0}^2 + C_{ne}^2$, where C_{n0}^2 is a constant for the whole propagation path and C_{ne}^2 is zero except when passing the plume. The physical processes of turbulence are not separable like this, but as there is a difference of several orders of magnitude in the structure parameter this separation can be used to simplify the mathematics without introducing significant errors. The beam wander can then be written as

$$\begin{aligned} \left\langle \rho_c^2 \right\rangle &= \frac{4.34L^2}{D^{1/3}} \left(C_{n0}^2 \int_0^L \left(1-\frac{\eta}{L}\right)^{5/3} d\eta + \int_{L-Z}^{L-Z+l} C_{ne}^2(\chi)\left(1-\frac{\eta}{L}\right)^{5/3} d\chi \right) \approx \\ &\approx 4.34\left(\frac{L}{D}\right)^{1/3} \left(\frac{3L^{8/3} C_{n0}^2}{8} + Z^{5/3} \int_0^l C_{ne}^2(\xi)\, d\xi \right) \end{aligned} \qquad (2)$$

where Z is the distance from the start of the plume to the screen and l the length (width) of the plume with the assumption l<<Z.

As the air surrounding the experiment setup is disturbed by the air-flow from the engine we assume a relatively high value of $C_{n0}^2 = 10^{-13}\ m^{-2/3}$ in our calculations, but even for this value the influence is negligible. For the longitudinal propagation we have L=86 m, Z=75 m and D=5 mm. Substituting these numbers in (2) we find

$$\left\langle \rho_c^2 \right\rangle = 112\left(5.4\times10^{-9} m^2 + 1.3\times10^{3} m^{5/3} \int_0^l C_{ne}^2(\xi)\, d\xi\right). \qquad (3)$$

As C_{ne}^2 varies with an unknown functional dependence inside the plume we study the integrated value

$$I_C = \int_0^l C_{ne}^2(\xi)\, d\xi \qquad (4)$$

For the measured rms-deviations of 5.6-17.1 mm I_C varies from $2*10^{-10}$ to $2*10^{-9}$ $m^{1/3}$. In addition to the doubts of the validity of equation (1) the largest uncertainties are that the beam diameter D is not constant and not exactly known, and that the plume length l is not totally negligible compared with the propagation distance Z. The effective length of the plume where C_{ne}^2 is more than half of the peak value can be estimated to be a few metre, so we can state that the beam in the worst cases has passed through areas where the structure parameter is on the order of 10^{-9} $m^{-2/3}$. Sirazetdinov and coworkers found C_n^2-values of $1.6*10^{-9}$ $m^{-2/3}$ close to the nozzle and $2\text{-}5*10^{-10}$ $m^{-2/3}$ at a distance of 7 m from the nozzle[3]. It is not surprising that the experiments by Sirazetdinov give slightly larger values of C_n^2 than measured here as they used a full size engine, while we used a down-scaled engine test-rig. Our measurements were also performed three nozzle diameters away from the engine axis, where the turbulence is expected to be lower than closer to the engine axis.

The same approach can be used to derive the structure constant from the measurements with the laser beam propagating perpendicularly through the highly turbulent plume region. In this case the total propagation length was 22.1 m and the distance Z from the engine plume to the screen was 20.7 m. The laser beam diameter D was estimated to be 2 mm. For the perpendicular measurements it is justified to assume that the downstream airflow from the engine is not significantly affecting the atmospheric part of the propagation path. Therefore the structure constant C_{n0}^2 can be derived from measurements with engine turned off. Values in the magnitude of 5.6×10^{-14} to 8×10^{-14} $m^{-2/3}$ can be found. Nevertheless the influence of this value using equation (2) to obtain the plume structure parameter C_{ne}^2 is negligible. The value for C_{ne}^2 derived from the measured standard deviation of the radial beam centroid deflection shows almost no dependence on C_{n0}^2.

The 1 to 2.5 mm centroid deviations that were measured correspond to I_C-values of 6.7×10^{-11} to 3.9×10^{-10} $m^{1/3}$. No significant difference of I_C is found when comparing values obtained from measurements with the beam passing at 1.9 m or 4.05 m downstream from the nozzle. The transverse profile of the refractive index structure parameter is expected to be symmetric and it is thus reasonable to define an effective top hat distribution. The only measured value is however I_C and the factoring into effective plume diameter Δ and structure parameter has to be made arbitrarily. Using a standard deviation of the radial beam centroid deflection of 1.43 mm, which corresponds to the engine running at full power with the beam passing 4.05 m downstream from the nozzle, we derive a C_{ne}^2 of 7.0×10^{-10} $m^{-2/3}$ for Δ=20 cm and 2.7×10^{-10} $m^{-2/3}$ for Δ=50 cm, respectively. It is reasonable to believe that the plume broadens as it gets further away from the nozzle and the almost constant integrated structure parameter I_C for our two experimental geometries would thus mean that C_{ne}^2 decreases, something that also seems intuitive. It is interesting to note that while we see very small difference in the measured beam wander at the two positions using this method the wave front sensor measurements showed a big decline in the wavefront aberration between the two positions used there.

The movement of the average spot positions of the blackbody and the laser beam in the images taken through the plume is attributed to refraction. The hot plume creates a strong temperature gradient. The hot gases near the centre of the plume will have a lower density and therefore a lower index of refraction. This will cause light rays to bend away from the hot regions. The observations can be explained qualitatively by the scheme indicated in Figure 14. The solid lines indicate the straight propagation in the absence of a temperature gradient. The dashed lines show the situation for a temperature gradient, occurring when the engine is on. The black body will continue to emit in all directions, but now because of the refraction effect, only the emission following the curved path will reach the camera. Effectively this will be “seen” by the camera as a ray coming from a position below the real black body position. This results in a downward shift of the observed black body position in the image. The laser beam is pointed parallel to the plume centre line and remains parallel when the engine is off. As a result of the refraction when the engine is switched on, the laser beam curves upwards and the laser spot location moves up in altitude. However, the reflected laser light as seen by the camera will be observed at a

lower position than the true position, following the same reasoning as for the black body. This partial compensation of the upward displacement has been observed in the experiments (Figure 9). That the compensation is not perfect is an effect of the parallax between the laser and the camera, and of the difference between beam wander of a collimated beam and angle of arrival of a spherical wave.

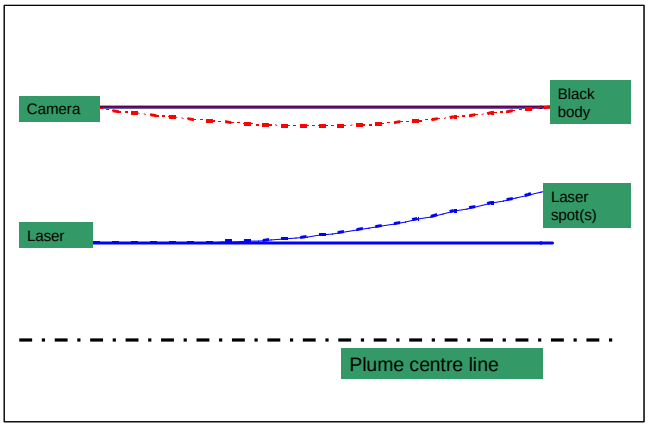

Figure 14. Illustration of optical paths with engine off (solid) and engine on (dashed) showing the compensation of laser beam displacement and tracker angle of arrival.

Wave front sensing with a Shack-Hartmann setup was used for characterizing the induced optical effects and for documenting the statistics of the optical degradations because of the turbulence of the plume. The measured data were also intended as comparison data or input data to simulation codes for laser beam propagation along the plume. Analysis was done at two different points downstream the nozzle so as to make measurements through quite different turbulent regions within the plume. The analysis were performed across the plume at 1142 mm and at 3500 mm downstream the nozzle, where the turbulence was supposed to be in a state between laminar and turbulent close to the nozzle and then fully developed further downward.

The worst turbulent conditions occur at the analysing point close to the nozzle. Then the PSD's degradations drop by one decade between the measuring point close to the nozzle and the downward observing point. The beam wander effect associated with the tip-tilt coefficients is by far the most degrading turbulent effects. The wave front measurements were performed at 80 mm above the nozzle plume main axis, that is close to the outer border of the plume, so that the turbulence created by the mixing of the air injected along or surrounding the plume and the hot air of the plume contains large scale structures at the origin of the observed beam wander. This property was confirmed when comparing the directly computed rms values of the overall wave front degradations with the rms values calculated with the tip-tilt component removed.

5 Discussion on experimental techniques

Characterization of the turbulence field behind an engine is a very difficult problem. The high wind speeds and accompanying rapid variation of turbulence and small turbulence cells put very high demands on temporal bandwidth and spatial resolution of the measurement systems. The main problem is, however, the limited access to the experimental facility. As the engine is relatively expensive to run experiments can only be performed a small number of times and each time during a short duration. Because of safety regulations, it is also mostly impossible to access the measurement equipment while the engine is running. There are also a number of constraints on how the equipment can be positioned around the engine. These limitations apply not only to the engine test rig used for the trials described in this report, but in general for all aircraft engines even though the constraints may be slightly different depending on which engine is used.

Imaging of the laser spot after the beam has propagated through the turbulence behind the engine is a simple way of obtaining information about the path-integrated turbulence effects. Parameters that are interesting and simple to analyze are magnitude and temporal statistics of the instantaneous deflection of the centre of gravity, as well as the long-term spot size. It is also possible to analyze the power in the bucket, the energy incident in a certain aperture, by integrating over a software aperture in the image. Together these measurements can give much information on how the turbulence affects system performance, as they are similar to the important performance measures for operative systems.

There are a number of problems remaining in the interpretation of the measured data to real system performance. The foremost is the lack of knowledge about how the effects scale with engine parameters. Other concerns are that the scintillations were not fully developed as the measurement geometry did not allow propagation to the true far field, and that the laser beams had smaller diameters and larger divergence than what is envisioned for operational systems on aircraft.

The Shack-Hartmann technique for measuring the perturbed wavefront was used for the first time for measurement through a turbulent plume downstream an engine nozzle. Knowledge of the wavefront disturbances can give a lot of information on the physics of the turbulence field. The technique, now in common use in adaptive optical system in the turbulent atmospheric problem, is more recently in use also in wind-tunnel investigations. In such severe environments, the technique has demonstrated its capability to provide accurate measurements despite occurrence of vibrations, which can be a major drawback. This is partly a result of the ability of the Shack-Hartmann technique to subtract a reference. The experience from the earlier wind tunnel trials allowed the ONERA team to use this technique successfully under the difficult conditions that exist close to the jet engine.

All the runs conducted at VAC with various engine states provided many series of raw wave front slopes, each series being associated with a set of various parameters (distance from nozzle and engine status). Collected data were then submitted to a Fourier analysis to derive the spatial power spectra densities (PSDs) of the degraded wave fronts, which is an appropriate function to infer the statistical effects of the optical turbulence: magnitude of the degradation per spatial frequency, particular power laws according to frequency domains and associated spatial frequencies, inertial sub-domains.

The obtained wave front PSDs scale accordingly with increasing values of the engine power parameters. The degradation is much lower, as expected, whenever just free stream is running. These consistently observed tendencies provide confidence in the wave front sensing performed at VAC.

One important type of measurement equipment that was lacking during these trials was sensors to measure the local turbulence in one point. All sensor systems present integrate the effects along the propagation path, and reversing this integration to determine the

refractive index variations along the path are in general not possible. Different types of anemometers that measure the variation of wind speed and temperature in a single point could add a lot to the knowledge of the turbulence behind an engine. Performing this kind of measurements is, however, not simple because of the high average wind speeds and high temperatures in the plume.

6 Discussion regarding implications on system performance

From equation (2) a comparison between the beam-wander effects caused by the plume and by the propagation through the free atmosphere can be made. With a laser placed on the aircraft Z≈L and the plume effects will thus dominate if

$$\int_0^l C_{ne}^2(\xi)\,d\xi > \frac{3LC_{n0}^2}{8}. \qquad (5)$$

As the propagation path through the disturbed region is at least a few metres for a full-scale engine with the laser beam propagating longitudinally or diagonally to the engine axis and the turbulence strength in the atmosphere is very low at higher altitudes the plume effects will dominate totally for the relevant propagation distances of a few kilometres. The beam wander contribution from the atmosphere can thus be neglected, but other sources of beam wander as laser pointing jitter, mechanical vibrations and aero-optic effects around the fuselage may still need to be taken into account.

Compensation for the laser-pointing error through the plume is provided automatically to some extent. The tracking camera of the pointing system will look through the same inhomogeneous plume as through which the laser is pointed. This means that the observed position of the target is shifted over a comparable angle as the error angle in the laser pointing induced by refraction. In a pointing and tracking system, the shift in observed position of the target towards the plume will result in shift in the laser pointing angle in the same direction. When the angular deflection for the laser beam is exactly equal to the shift of the target position, the laser will be pointed at the target. Since the gradient in the refractive index is not uniform, this compensation mechanism is only correct when the tracker and laser pointer are exactly on the same optical axis and have the outgoing beam diameter matched to the width of the collecting aperture of the tracker. The different apertures of averaging the tilt will produce a difference in perceived tilt. As in general, the laser-beam diameter is smaller than the tracker aperture the laser will experience larger tilts that vary more rapidly.

Taking the measured temporal statistics of the laser beam wander into account we see correlation times on the order of 3.5 ms. This means that we should either use a relatively slow tracker, which is matched to the expected angular speed of the target, or a very fast tracker with sub-millisecond latency times from position measuring to pointing correction, to avoid introducing additional pointing errors with the tracker.

Another complicating factor might be introduced by the fact that the fluctuations in the positions observed for an extended target, such as a missile plume, will not be fully representative of fluctuations over the narrow optical path for the laser beam. It is expected that owing to spatial averaging effects, the observed position of an extended target will show smaller fluctuations than those expected for a point source. Thus the fast variation will always be underestimated and total compensation by pointing in the direction measured by the tracker will not be achieved.

The rapid beam wander not compensated by slow trackers showed rms amplitudes of up to 350 µrad in these measurements. A first attempt at scaling the magnitudes to a full-size engine (that has not been validated) is to scale the perturbations linearly with nozzle diameter. As the nozzle diameter in these tests was 10 cm we can expect anywhere from 2 to 10 times larger effects in real aircraft depending on type. From an application point of view the issue is to point the laser beam on a missile seeker aperture with less than 10 cm diameter at km distances. Consequently, the cone where the laser beam will hit the intended target is smaller than 100 µrad. The realistic range of beam divergences for a DIRCM system is 400 µrad to 1 mrad, with the lower limit set by aperture diameter (and beam quality) and the upper by the available power.

Moreover, the beam will be distorted and broken up by the turbulence, but the short-term spot will not cover a significantly larger area than the undisturbed beam. Taking these tentative figures into account, it is clear that the beam may in a large number of cases totally miss the seeker aperture and there will be drop-outs in the jam code. The end result will probably be that jamming with a DIRCM system through the central parts of the engine plume will not give totally effective protection against heat-seeking missiles and break-lock may be delayed slightly. The extent of the region of reduced laser based DIRCM system performance depends on the type of engine and of the relative positioning of the DIRCM turret relative to the engines.

7 Conclusion

Measurements of the laser beam wander after propagation through the plume behind the jet engine have been performed. The beam deflection can be estimated if we assume that all refraction takes place in the plane of the nozzle, an approximation that is acceptable as the distance to the measurement position was large compared to the extent of the plume. Beam deflections of up to 350 μrad (rms) were measured, and variation with engine thrust and distance from the engine axis was observed.

Laser beams propagating across the plume were imaged and measured with a Shack-Hartmann wave-front sensor. The collected wave-front data and their statistical interpretation reveal some interesting physical properties about the turbulent contributions of the traversed region. These local properties are also of interest for the simulation of the propagation of a laser beam along the plume. More precisely, the original measured wave-front data can be used to validate the models developed in the WP3 for simulating the laser propagation along the plume.

The observed turbulence effect magnitudes are such that even for the down-sized jet-engine test rig that was used for these trials the turbulence from the plume would be much stronger than the natural atmospheric turbulence for relevant propagation distances and the impact on DIRCM system efficiency would be severe in some limited pointing directions. Scaling to actual aircraft sized engines is expected to increase the scale of effects and jamming of missile seekers through the centre of the engine plume may be challenging.

In summary, the experimental study regarding laser beam propagation through air disturbed by jet engine exhaust plumes have shown that severe perturbations may be induced in the laser-beam pointing and target-tracking capabilities. Further studies are required to extrapolate the observed effects for the model engine to full-scale engines. Another important issue is related to other platforms such as helicopters and transport aircraft using turboprop engines. In these cases the influence from engine related perturbations on laser beam propagation and tracking needs to be investigated and the impact on the installed performance assessed.

References

1. L. Sjoqvist, "Laser beam propagation in jet engine plume environments: a review," Proc. SPIE, **7115**, pp. 71150C-71115 (2008).

2.C. Chen, and W. Rodi, "Vertical turbulent buoyant jets: a review of experimental data," NASA STI/Recon Technical Report A **80**, 23073 (1980).

3.V. S. Sirazetdinov, "Experimental study and numerical simulation of laser beams propagation through the turbulent aerojet," Applied Optics **47**, 975-985 (2008).

4.C. B. Hogge, and W. L. Visinsky, "Laser beam probing of jet exhaust turbulence(Structure constant of jet exhaust turbulence of J-57 with afterburner by laser beam probing compared with scintillation and hot-wire anemometer measurements)," Applied Optics **10**, 889-892 (1971).

5.J. L. Barrett, and P. A. Budni, "Laser beam propagation through strong turbulence," Journal of Applied Physics **71**, 1124 (1992).

6.D. H. Titterton, "Measurement of the Distortion Generated in a Laser Beam's Characteristics Resulting from Passage through an Engine's Wake," in *RTO SET Symposium E-O Propagation, Signature and System Performance under Adverse Meteorological Conditions Considering Out of Area Operations*(Naples, 1998), pp. RTO MP-1.

7.W. M. Isterling, L. J. Cox, M. Dubovinsky, D. H. Titterton, and T. Porter, "Laser Interaction with Jet Engine Exhaust Induced Turbulence," Proceedings of the 4th Australian Conference on Laser Diagnostics in Fluid Mechanics and Combustion (2005).

8.W. M. Isterling, L. J. Cox, M. Dubovinsky, D. H. Titterton, and T. Porter, "Laser beam propagation through a jet engine exhaust," in *AOC International Symposium and Exhibition, 13 - 14 February 2006, Adelaide, Australia*(2006).

9.L. Sjoqvist, O. Gustafsson, and M. Henriksson, "Laser beam propagation in close vicinity to a down-scaled jet engine exhaust," Proc. SPIE **5615**, 137-148 (2004).

10.M. Henriksson, L. Sjoqvist, and O. Gustafsson, "Experimental study of mid-IR laser beam wander close to a jet engine exhaust," Proc. SPIE, **6397**, 639709 (2006).

11.M. Henriksson, L. Sjöqvist, D. Seiffer, N. Wendelstein, and E. Sucher, "Laser beam propagation experiments along and across a jet engine plume," Proc. SPIE **7115**, pp. (2008).

12.R. Deron, and F. Mendez, "Characterization of optical turbulence in a jet engine exhaust with Shack-Hartmann wavefront sensor," Proc. SPIE **7115**, pp. 71150F-71112, (2008).

13.M. Henriksson, L. Sjöqvist, O. Gustafsson, and M. Elmqvist, "Laser beam progatation and active imaging experiments close to a jet engine plume," FOI Report, FOI-R--2529--SE (2008).

14.H. M. A. Schleijpen, "Laser pointing in the vicinity of jet engine plumes," Proc. SPIE, **7483**,.pp. 74830E-74830E-11, (2009).

15.F. Smith, "Atmospheric propagation of radiation," The infrared and electro-optical systems handbook-IR/EO systems handbook, Bellingham: SPIE-The International Society for Optical Engineering and Ann Arbor, Michigan: ERIM-Infrared Information Analysis Center,| edited by Smith, Frederick G. (1993).